Journal of Power Sources 243 (2013) 354–360

Contents lists available at SciVerse ScienceDirect

Journal of Power Sources

journal homepage: www.elsevier.com/locate/jpowsour

Entropy change effects on the thermal behavior of a $LiFePO_4$/graphite lithium-ion cell at different states of charge

K. Jalkanen, T. Aho, K. Vuorilehto*

Department of Chemistry, School of Chemical Technology, Aalto University, P.O. Box 16100, 00076 Aalto, Finland

HIGHLIGHTS

- $LiFePO_4$/graphite lithium-ion cell cools down during discharge.
- Cooling effect was calculated from the potentiometric entropy change measurement.
- The same cooling effect was also confirmed calorimetrically.
- Both a commercial full cell and its individual electrode materials were studied.
- The full cell graphite/$LiFePO_4$ ratio is determined for result interpretation.

GRAPHICAL ABSTRACT

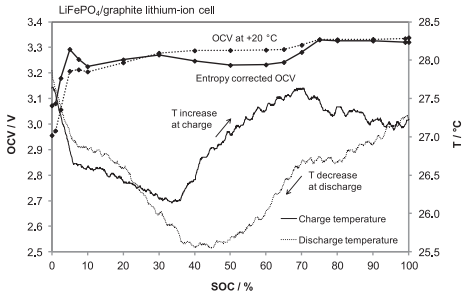

ARTICLE INFO

Article history:
Received 12 March 2013
Received in revised form
23 May 2013
Accepted 28 May 2013
Available online 13 June 2013

Keywords:
Lithium-ion cell
Entropy
Cooling
Lithium iron phosphate
Graphite

ABSTRACT

The enthalpy and entropy changes in a commercial lithium-ion cell were studied by using potentiometric measurements. The experiments were done on the full cell and individually on its electrode materials, $LiFePO_4$ and artificial graphite. The graphite electrode entropy change follows the amount of intercalated lithium, whereas the LFP electrode entropy change is independent of the lithium content. The full cell entropy change behavior can be concluded to originate from the graphite electrode. For the states of charge between 30 and 75%, the full cell entropy change is positive in the discharge direction, causing the cell to absorb heat. Thus when low discharge currents are used, this entropy effect dominates over the irreversible, heat producing losses, and as a result the cell cools down. In the charge direction the entropy change has the same absolute value but is negative in sign. Because of this, the cell produces extra heat in addition to the irreversible heat production, and thus warms up. These phenomena were confirmed in a calorimetric experiment. The thermal behavior results can be utilized in designing the battery pack cooling system and in choosing favorable states of charge for the battery cycling.

1. Introduction

In recent years, the application area of lithium-ion batteries has expanded from small consumer electronics, such as mobile phones, to large systems, including electric vehicles, industrial machines and stationary energy storage applications. These large-size applications utilize lithium-ion battery packs consisting of up to hundreds of large-format single cells. Due to the higher energy content, a potential malfunction results in more serious consequences. This fact emphasizes the importance of understanding and investigating the battery thermal behavior at the cell level for assuring safe use of the battery pack. Also the inherent safety of the electrode materials plays a bigger role. Lithium iron phosphate (LFP) has become one of the choices for the positive electrode, replacing more dangerous lithium cobalt oxide (LCO). Unlike LCO, LFP is considered to be thermally stable, which makes it a very reasonable material for large-size applications.

* Corresponding author.
E-mail address: kai.vuorilehto@helsinki.fi (K. Vuorilehto).

0378-7753/$ – see front matter © 2013 Elsevier B.V. All rights reserved.
http://dx.doi.org/10.1016/j.jpowsour.2013.05.199

Depending on the battery size and application, the battery packs usually have to include active cooling. When the battery pack size increases, the area-to-volume ratio decreases, and the heat transfer away from the battery becomes more inefficient. Depending on the heat generation rate in the individual cells, air cooling or more effective water cooling is needed. To be able to scale the needed cooling system, the heat generation rate of the cell has to be determined. The total heat generation rate consists of reversible and irreversible parts. The irreversible heat generation rate only depends on the current and internal cell resistance, whereas the reversible one is a function of the entropy changes in the electrode materials during the cell reactions. The entropy change reflects the way lithium-ions are ordered in the electrode material lattices. A positive entropy change is an indication of increasing disorder in the material as charge is passed through, while a negative one implies ordering. The entropy change typically depends on the lithium-ion content of the electrode material and thus the cell state of charge (SOC). This results in some SOC ranges being more favorable in terms of smaller absolute value of entropy change and thus less heat generation during the cell reactions. As the batteries are often used only within a narrow SOC range (micro cycling) instead of full cycles, this is valuable information for determining the preferable cycling range.

The entropy change of commercial lithium-ion batteries and individual electrode materials have been presented in the literature. Studies on the individual electrode materials have been done for both the LFP materials [1–3] and graphite material [4–7]. Also studies combining commercial full cells and measurements on their individual electrode materials have been done [1,7,8], but the combination of LFP and graphite is less studied. In this study, however, the LFP and graphite materials are investigated both in a commercial full cell as well as individual electrodes. The point to emphasize is that the electrode materials tested here separately were exactly the same as used in the full cell. This is highly advantageous as it has been observed that the material synthesis process significantly affects the measured entropy change values of an electrode material [7]. Another important feature of this study is that the negative to positive electrode ratio of the full cell could be determined. To prevent lithium plating, commercial lithium-ion cells having graphite negative electrode always have an excess of the graphite material compared to the positive electrode. Knowing the graphite/LFP ratio enables the exact division of the cell performance to the different electrode contributions and a more precise interpretation of the cell behavior and its origin.

The entropy change can be measured calorimetrically or potentiometrically. In this work, the potentiometric method was used, but also a qualitative calorimetric measurement was done to confirm the results and conclusions. Potentiometric measurements are severely affected by the possible self-discharge of the full cell or electrode materials, introducing a large error to the results. Other authors [3,8,9] have claimed that self-discharge indeed has been a problem and suggested corrections for it. In this study, however, no sign of self-discharge was observed and the potentiometric measurements can thus be considered to be very accurate. As for calorimetric measurements, they suffer from inaccuracy if the measured system has a large, inactive thermal mass. As lithium-ion cells always have many inactive parts, including the cylinder or pouch package, current collector tabs etc, which do not participate in the cell reaction, this could be problematic.

In this work, the entropy change of a commercial LFP/graphite full cell is divided into contributions of the LFP and graphite electrodes. Because of the entropy effect, the full LFP/graphite cell actually absorbs heat and thus cools down when it is discharged at low enough current in the SOC range of 30–75%.

2. Thermodynamic relations of a lithium-ion cell

The total heat generation rate Q_{total} of a cell is a measure of the amount of heat transferred from the surroundings to the cell. It consists of two parts:

$$Q_{\text{total}} = Q_{\text{irreversible}} + Q_{\text{reversible}} \tag{1}$$

Here the heat generation rates are given in watts. For an exothermic cell reaction, heat is transferred from the cell to the surroundings. This direction of the heat flow is defined here as a negative heat generation rate. The irreversible heat generation rate $Q_{\text{irreversible}}$ depends on the current value I and on the cell internal resistance R_{i} as follows:

$$Q_{\text{irreversible}} = -I^2 R_i \tag{2}$$

The reversible heat generation rate $Q_{\text{reversible}}$ depends on the current value and its sign, and also on the entropy change ΔS as follows [1,7]:

$$Q_{\text{reversible}} = T\Delta S\frac{I}{nF} \tag{3}$$

In this work, the discharge current is determined to be positive. $Q_{\text{irreversible}}$ is always associated with heat production; it is exothermic and negative in sign for both charge and discharge. $Q_{\text{reversible}}$, however, can be either positive or negative for the same cell reaction direction, depending on the sign of entropy change. Depending on the sum of $Q_{\text{irreversible}}$ and $Q_{\text{reversible}}$, the total heat generation rate Q_{total} is either positive or negative and the cell absorbs or evolves heat.

The entropy change of a cell reaction $\Delta S_{\text{full cell}}$ is the sum of the positive and negative electrode contributions, ΔS_{LFP} and $\Delta S_{\text{graphite}}$. It is here given for the full cell discharge direction, which corresponds to a reduction reaction at the positive electrode and oxidation reaction at the negative electrode. However, the measured values for the negative electrode are for the reduction reaction and must be thus reversed in sign:

$$\begin{aligned}\Delta S_{\text{full cell,discharge}} &= \Delta S_{\text{LFP,reduction}} + \Delta S_{\text{graphite,oxidation}} \\ &= \Delta S_{\text{LFP,reduction}} - \Delta S_{\text{graphite,reduction}}\end{aligned} \tag{4}$$

The entropy change of the cell reaction can be related to the cell open circuit voltage (OCV) through the equation for Gibbs free energy change ΔG. The Gibbs free energy change is given by [8,10]:

$$\Delta G = \Delta H - T\Delta S \tag{5}$$

where ΔH is the enthalpy and ΔS the entropy change of the cell reaction. The Gibbs free energy change can also be expressed as follows [10]:

$$\Delta G = -nF(\text{OCV}) \tag{6}$$

where n is the stoichiometric number of electrons participating in the cell reaction (for a lithium-ion cell, $n = 1$). By combining equations (5) and (6) it is seen that the measured OCV values consist of enthalpy and entropy terms and can be expressed as:

$$\text{OCV} = -\frac{\Delta H}{F} + \frac{T\Delta S}{F} \tag{7}$$

Equation (7) can be applied to determine the enthalpy and entropy change values from the cell OCV recorded at different temperatures. The entropy and enthalpy changes can be calculated from the OCV vs. temperature-data as follows:

$$\Delta S = F\frac{\partial(\mathrm{OCV})}{\partial T} \tag{8}$$

$$\Delta H = F\left[T\frac{\partial(\mathrm{OCV})}{\partial T} - (\mathrm{OCV})\right] = -F[(\mathrm{OCV})]_{T=0\ \mathrm{K}} \tag{9}$$

When low currents are used and the internal resistance of the cell is small, the total heat generation rate mainly consists of the reversible part. Thereby the entropy change determines whether heat is absorbed or evolved. The cell OCV consists of enthalpy and entropy terms, according to Equation (7). The cell thermal behavior evaluation can be done by comparing the measured OCV and an entropy corrected OCV, which is defined by:

$$(\mathrm{OCV})_{\text{Entropy corrected}} = -\frac{\Delta H}{F} \tag{10}$$

The difference between the OCV and the entropy corrected OCV is due to the entropy effect. A positive entropy change causes cooling during discharge and heating during charge.

3. Experimental

A commercial lithium-ion cell provided by European Batteries Ltd. was used for the full cell measurements. The cell was a prismatic, pouch-type cell with a nominal capacity of 42 Ah. The positive and negative electrode materials used were LFP (P1 Clariant, Canada) and graphite (artificial type), respectively.

Electrochemical test cells (ECC-Std, EL-Cell, Germany) of 18 mm diameter were used to individually test the electrode materials as half-cells. The electrode samples were received from European Batteries Ltd. and they were exactly the same materials as used in the commercial cell tested in this study. The counter electrode was metallic lithium (Sigma–Aldrich, thickness 0.75 mm, 99.9% trace metals basis) and a glass fiber separator of 0.65 mm thickness (provided by EL-Cell) was used. The electrolyte solution was received from European Batteries Ltd. and it was the same as used in the commercial cells consisting of 1 M $LiPF_6$ as conducting salt in a quaternary mixture of ethylene carbonate (EC) and other common organic carbonates.

Charging and discharging of the cells was performed using a Maccor battery cycler (Maccor 4300, USA). Prior to the potentiometric measurements, both the full cell as well as the half-cells were cycled at a very slow 0.03C rate for one cycle to determine the actual capacity, which is needed for precise adjustment of the cell SOC. The cut-off voltages used in cycling and later in adjusting the cell SOC are presented in Table 1. It is to be noticed that in a graphite half-cell, graphite is the more positive electrode and the movement of lithium-ions from the lithium counter electrode to the graphite electrode by definition corresponds to discharge. In this work, however, this cell reaction direction is referred to as charging, in order to be consistent with the situation in a full lithium-ion cell.

The potentiometric measurements were performed in a temperature chamber (ESPEC, model BTZ-175E). The chamber had active air circulation to ensure constant and accurate temperature condition throughout the OCV measurements. The tested cell was adjusted to the desired SOC at +20 °C temperature using 0.1C constant current. The 100% SOC was defined as a constant current charge until the charge cut-off voltage was reached followed by a constant voltage charge until the current reduced to 0.03C. Correspondingly, the 0% SOC was defined as a constant current discharge until the discharge cut-off voltage followed by a constant voltage discharge until the current reduced to 0.03C. In the full cell, the graphite negative electrode is in excess and thus the graphite lattice is never completely full of lithium and the graphite electrode itself never reaches 100% SOC.

After the desired SOC was reached, the cell was left to stabilize for 20 h at +20 °C temperature in order to reach equilibrium. To measure the dependence between OCV and temperature, the chamber temperature was first decreased to 0 °C, and left to stabilize for 2 h. After that, the temperature was increased by 10 °C steps with a stabilization time of 1.5 h until the temperature of +40 °C was reached. Finally, the temperature was set back to +20 °C for 2 h. The OCV of the cell was registered at 20 s steps during the whole procedure. The OCV value for each temperature was taken as the average of the recorded values for the last 30 min, where the OCV was considered to have stabilized. This test regime was repeated for several SOCs for both the full cell as for the half-cells and is presented in Fig. 1.

In the half-cell experiments, the entropy and enthalpy changes are measured between an LFP or graphite working electrode and a lithium counter electrode. During the cell reaction, lithium is dissolved from or precipitated on the metallic lithium counter electrode, whereby the lithium electrode composition or the chemical environment of the lithium atoms in it does not change. Thus it can be assumed that all the observed entropy and enthalpy differences between different SOCs are only due to the changes in the LFP or graphite material investigated [1,4,5]. The contribution of the lithium metal also cancels out when combining the half-cell results for calculating the entropy change of the LFP/graphite cell from Equation (4). In addition to this, comparison of the results with literature data can be done with good accuracy, since lithium is commonly used as counter electrode for half-cell experiments.

To confirm the potentiometric results, a qualitative calorimetric experiment was done for the full cell. The cell was placed inside 50 mm thick styrofoam and cycled with 0.1C constant current using the same cut-off voltages as presented in Table 1. The cell temperature changes were recorded with a thermocouple attached on the cell surface.

Table 1
Cut-off voltages for cycling.

	Charge cut-off voltage/V	Discharge cut-off voltage/V
Full cell (LFP vs. graphite)	3.65	2.5
LFP half-cell (LFP vs. lithium)	4.0 (vs. Li/Li^+)	2.7 (vs. Li/Li^+)
Graphite half-cell (graphite vs. lithium)	0.01 (vs. Li/Li^+)	0.6 (vs. Li/Li^+)

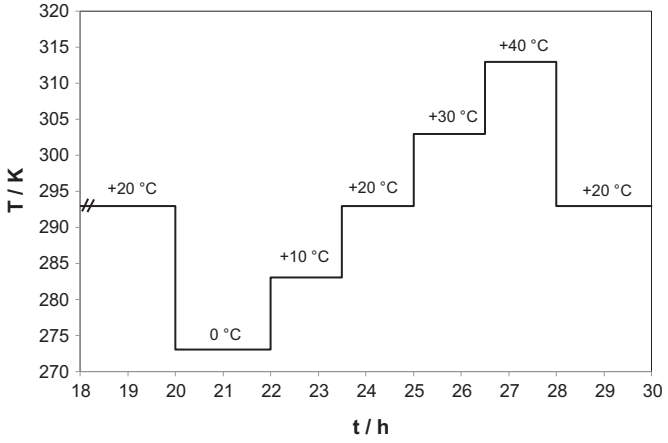

Fig. 1. Test regime for the temperature scanning in potentiometric measurements.

4. Results and discussion

The LFP and graphite half-cell voltages as well as the full cell voltage measured before the potentiometric experiments at 0.03C rate are shown in Fig. 2.

It can be seen from Fig. 2(a) that the LFP electrode potential stays almost stable over the whole SOC range. Between the almost full and empty compositions, in respect of the lithium-ion content, LFP material has a two-phase structure consisting of $LiFePO_4$ and $FePO_4$ phases, and the electrode reaction is a two-phase reaction between these phases with a varying total lithium concentration. The electrode potential remains almost constant inside the two-phase region although the ratio of the two phases changes [2,11]. However, rapid decrease or increase in electrode potential is observed near the SOC values of 0% (lattice almost full of lithium-ions) and 100% (lattice almost empty of lithium-ions), respectively. LFP has a low electrical conductivity and also the lithium-ion diffusion is slow in its lattice [12–14]. These material properties cause the difficulties to insert or extract the last lithium-ions into or from the LFP electrode and give rise to the observed potential behavior at the ends of the SOC range.

The graphite electrode potential on the other hand changes significantly as function of the SOC, as seen in Fig. 2(b). This is caused by the structure of graphite, where the lithium-ion intercalation takes place in an ordered way instead of random distribution between the graphene layers [15]. This phenomenon is called staging and the lithium-ion distribution is described with a stage number, which tells the number of graphene layers between the layers of intercalated lithium. The two-phase areas of co-existing intercalation phases are seen as plateaus and the single-phase areas as changes in potential [16]. The intercalation stages are the following as the lithium-ion concentration in graphite is increased: dilute stage-1, stage-4, stage-3, liquid-like stage-2 (2L), ordered stage-2 and ordered stage-1 [16].

In Fig. 2(c) the full cell voltage is shown, and based on the half-cell results in Fig. 2(a) and (b), it is evident that the changes in cell voltage are mostly caused by the graphite electrode. The cell voltage reflects the graphite electrode potential and thus it is affected by the effective graphite/LFP ratio. When a lithium-ion cell is assembled, all the active lithium-ions are brought to the cell with the LFP material and the graphite material is in excess. As the cell is formatted and cycled, a part of the active lithium is consumed at the graphite electrode to the solid electrolyte interface (SEI) layer formation. Thus the effective graphite/LFP ratio changes constantly and is to be determined just prior to the measurements. In graphite material, the stage-2 single-phase and the potential change related to it is theoretically found at 50% SOC [16]. If this potential change and the corresponding SOC value are determined from the full cell voltage curve, the excess amount of graphite with respect to LFP can be calculated. This is illustrated in Fig. 3, with measurement data taken from Fig. 2(b) and (c).

It is shown in Fig. 3 that the stage-2 single-phase is located at 52% SOC in the graphite half-cell. This differs slightly from the theoretical value of 50% SOC because not all the 372 mAh g^{-1} graphite theoretical capacity can be fully taken from the graphite half-cell. This means that the composition completely full of lithium-ions is not achieved and thus the stage-2 ↔ stage-1-plateau is shorter than expected. The same stage-2 single-phase is seen in the full cell at 70% SOC. Thus it can be calculated that the effective graphite/LFP ratio is 70%: 52%, which equals 1.35.

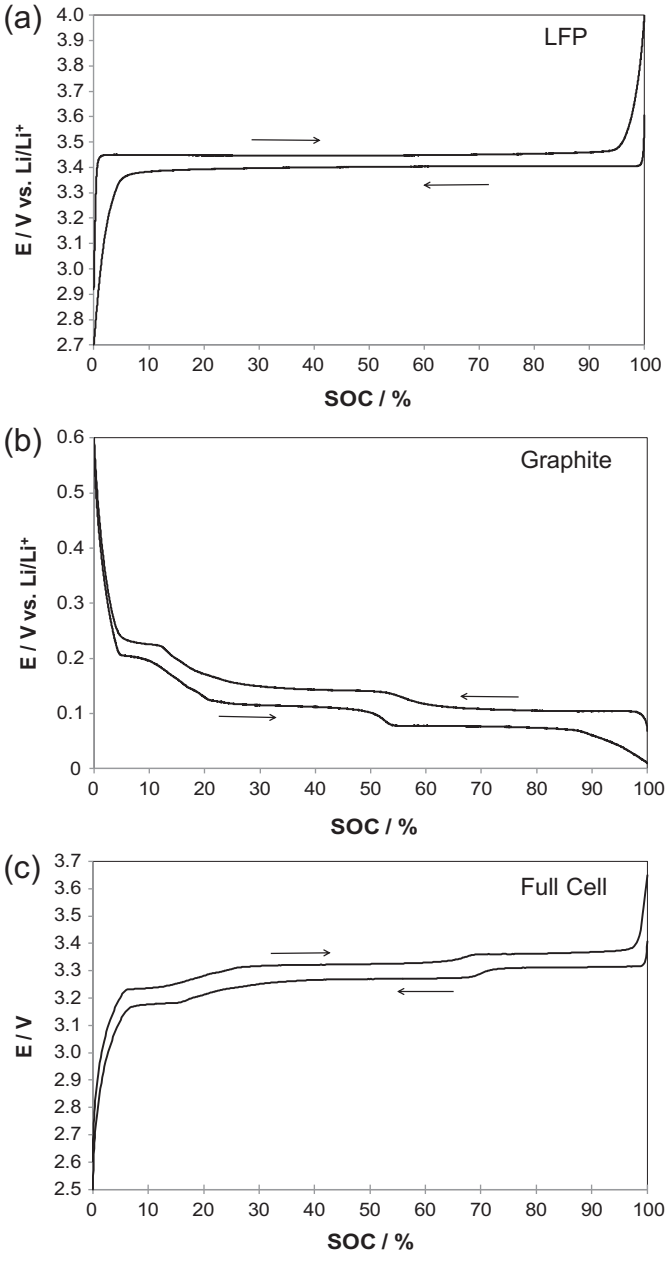

Fig. 2. Voltage as a function of SOC at 0.03C constant current. (a) LFP half-cell (vs. metallic lithium); (b) graphite half-cell (vs. metallic lithium); (c) full cell.

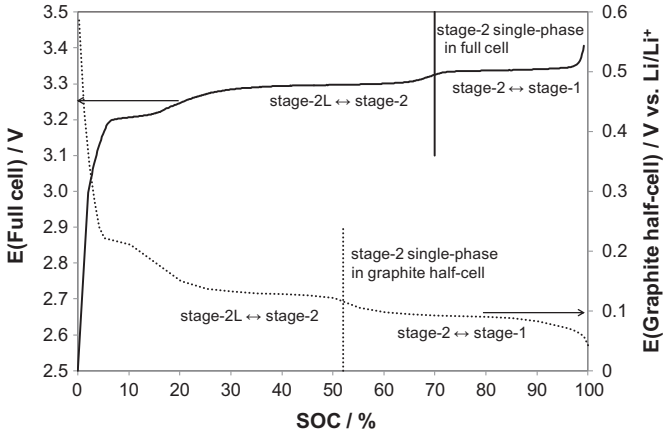

Fig. 3. Full cell and graphite half-cell voltages vs. SOC and graphite stage-2 intercalation SOCs (corresponding vertical lines).

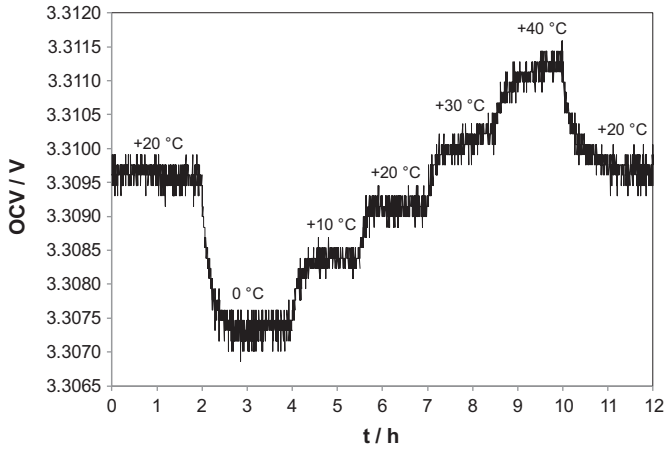

Fig. 4. Potentiometric measurement of the full cell at 70% SOC plotted as OCV vs. time.

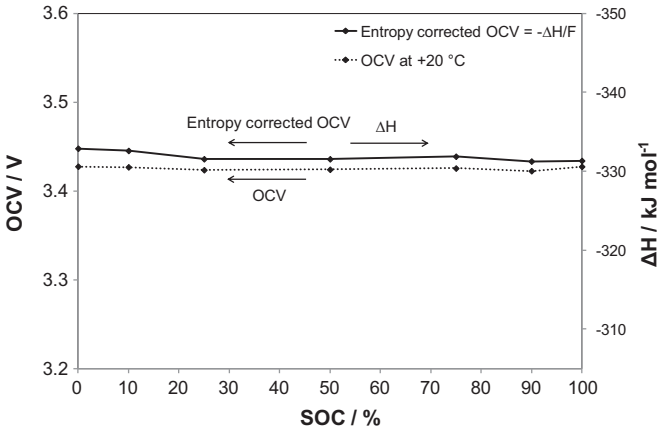

Fig. 6. Entropy corrected OCV (=−Δ*H*/*F*) and OCV at +20 °C for the LFP half-cell.

After the origins of the cell voltage and the graphite/LFP ratio have been determined, the results of the potentiometric measurements can be interpreted. A typical potentiometric measurement plotted as OCV and temperature vs. time is shown in Fig. 4.

As it can be seen from Fig. 4 for the full cell, there was almost no shift in the OCV value before and after the temperature scanning. This means that there is no self-discharge in the full cell and no correction is needed, in contradiction to some other studies [3,8,9]. For the half-cell experiments, the OCV-shift was in the order of 0.5 mV, which is also tolerable without any corrections. The relaxation of lithium distribution inside the electrode materials has been sufficient, which is seen as a stable OCV value before the temperature scanning.

For calculating the entropy and enthalpy changes, the average OCV value of the last recorded 30 min of each measured temperature was taken. According to Equation (7), the OCV and temperature have a linear relationship. Fig. 5 shows a plot of OCV vs. temperature with linear fitting, corresponding to Fig. 4.

The entropy and enthalpy changes can be obtained according to Equations (8) and (9): entropy change Δ*S* from the slope and enthalpy change Δ*H* from the value at absolute zero temperature ($T = 0$ K). The entropy corrected OCVs calculated from Equation (10) and the OCV values at +20 °C taken from the potentiometric measurements are shown in Fig. 6 for the LFP half-cell, in Fig. 7 for the graphite half-cell and in Fig. 8 for the full cell. The entropy changes of the LFP and graphite half-cells as well as the full cell are presented in Fig. 9.

From Figs. 6 and 9, the LFP material enthalpy and entropy change behavior and the OCV characteristics can be evaluated. The enthalpy change in Fig. 6 for LFP material was found to be almost constant. The entropy change in Fig. 9 was measured to be negative and nearly constant; only a slight upward slope for increasing SOC was observed at the ends of the SOC range.

According to literature, LFP has a two-phase structure and the entropy change is expected to be constant in the intermediate SOCs [3]. However, at the ends of the SOC range, a transition from a two-phase structure to a single-phase structure is postulated [2,3]. Viswanathan et al. [1] measured the entropy change of two different LFP materials. The results were very similar to the results in this study, with the exception that the other material showed a rather rapid entropy change increase near 100% SOC, reaching positive values. Dodd [3] measured clearly a more sloping behavior for the intermediate SOCs, but a similar upward trend with increasing SOC was observed. They also observed the entropy change at the ends of the SOC range to be changing more rapidly than in this study. Yamada et al. [2] obtained the most distinct entropy change behavior and anomaly with sharp spikes for the nearly full and nearly empty SOCs. The sharp changes near 0% and 100% SOC were explained by formation of single-phase regions [2,3].

It can be concluded that the most differences between these studies are observed at the single-phase SOCs. The phase change to

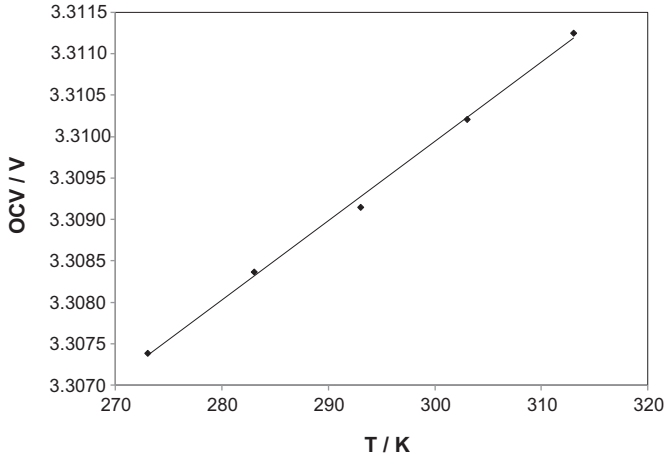

Fig. 5. OCV vs. temperature for the full cell at 70% SOC ($R^2 = 0.997$).

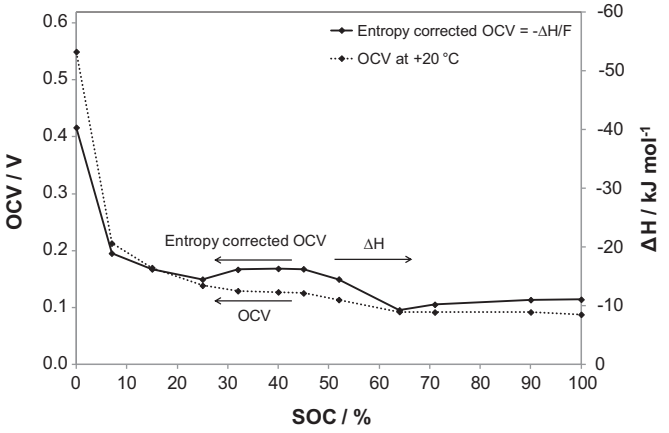

Fig. 7. Entropy corrected OCV (=−Δ*H*/*F*) and OCV at +20 °C for the graphite half-cell.

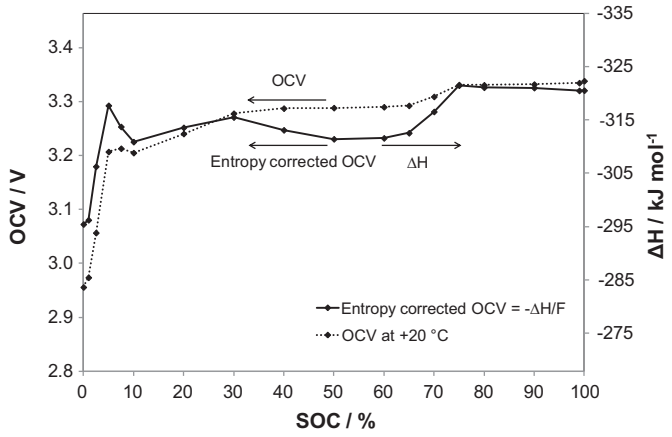

Fig. 8. Entropy corrected OCV ($=-\Delta H/F$) and OCV at +20 °C for the full cell.

the pure $LiFePO_4$ and $FePO_4$ compositions might be delayed. In addition, it is possible that due to the low conductivity of LFP not all the active mass is accessible and there are vacant sites even when the material is considered to be completely full of lithium. Differences in the LFP particle size [3], carbon coating and material purity might also cause some discrepancy. The shape of the entropy change vs. SOC has been found to be dependent on the material synthesis process [7] and this was also noticed for LFP in the study of Viswanathan et al. [1].

In graphite material both the enthalpy and entropy changes follow the staging process, which is observed in Figs. 7 and 9. An empty graphite lattice can be considered to be very ordered. Thus lithium intercalation leads to increasing disorder and is seen as positive entropy change at SOCs of 0–20%. After 25% SOC, there is a transition from more disordered stage-2L to ordered stage-2, which is expected to increase the ordering and indeed shows as a plateau of a negative entropy change. Just after the pure ordered stage-2 composition has been achieved, the entropy change shows a spike increasing to almost zero. Again, as more lithium is added, the entropy change shows another negative entropy change plateau at the transition from stage-2 to completely filled stage-1.

Similar characteristics as for the graphite investigated in this study were observed in other studies [1,4–7]. Until 20% SOC, the entropy change was measured to be positive and mainly sloping. Distinct plateaus of negative entropy change for the stage-2L ↔ stage-2 and stage-2 ↔ stage-1-transitions were observed. These transitions are known to be first-order phase transitions [16], for which the entropy change takes a constant value showing a plateau [6]. Also a spike for the pure stage-2 intercalation compound was noticed. The entropy change origins and division to configurational and vibrational entropy have been discussed in more detail by Reynier et al. [4,5].

The studied graphite materials included for example mesocarbon microbeads (MCMB) [5,6], natural graphite [5] and the artificial graphite of this study. The determining characteristic and the origin of the entropy change shape can thus be concluded to be the ordered, graphitic structure; disordered carbons show a very different behavior with a small entropy change, which is almost independent of lithium content [5].

When comparing the results in Figs. 6–9 it is evident that the SOC dependence of the full cell entropy change is determined by the graphite electrode. If the half-cell results are combined, the entropy change of the full cell can be calculated by using Equation (4), whereby the measured graphite electrode entropy change values are reversed in sign. This is shown in Fig. 10. The graphite SOC is adjusted to correspond to the graphite/LFP ratio in the full cell.

It is shown in Fig. 10 that the shape of the full cell entropy change curve vs. SOC corresponds to the half-cell results, although there is a slight deviation in the exact entropy change values. The only noticeable deviation in the results is seen between the SOC range of 40–70%, which corresponds to the stage-2L ↔ stage-2-transition at the graphite electrode. The phase diagram of graphite with intercalated lithium-ions shows temperature dependence with the stage-2L disappearing below +10 °C (±2 °C) [16]. This might have caused some error to the full cell and graphite half-cell results. Additionally, the SEI-layer formation consumes part of the active lithium, and thus the LFP electrode never reaches exactly 0% SOC (complete $LiFePO_4$-composition). This partly explains why the measured values in the LFP half-cell do not exactly correspond to the values in the full cell.

A qualitative calorimetric experiment was done to confirm the theoretical results in practice. The OCV at +20 °C and the entropy corrected OCV compared with the corresponding temperature results from the calorimetric measurement are shown in Fig. 11.

The entropy effect can be seen in Fig. 11 as deviation of the entropy corrected OCV from the OCV at +20 °C. When a low enough discharge current is used and the cell internal resistance is small,

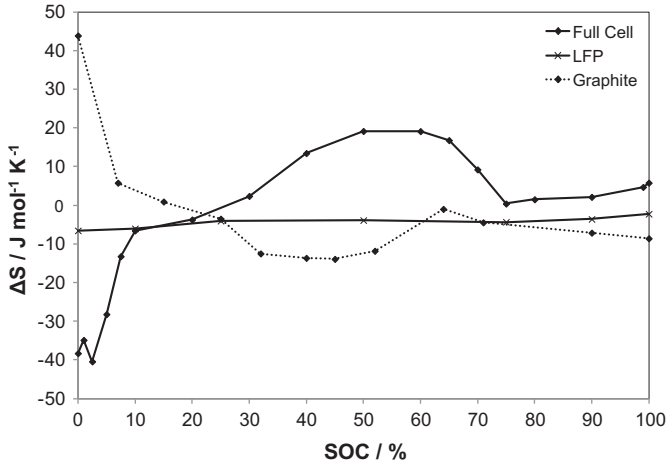

Fig. 9. Entropy change for the full cell, LFP half-cell and graphite half-cell. The graphite/LFP ratio of 1.35 has not been taken into account and therefore the SOCs of graphite in the full cell and in the half-cell do not correspond.

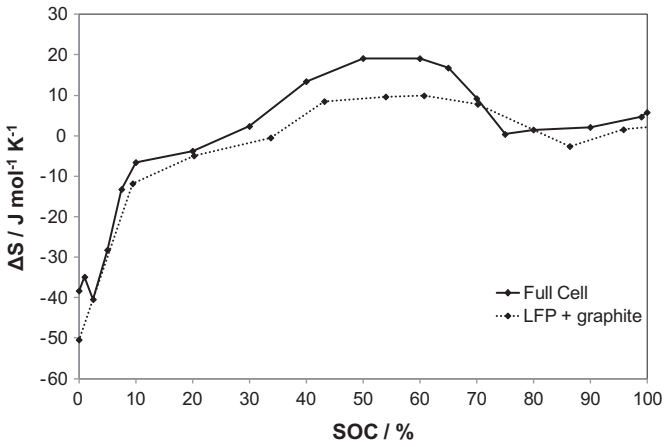

Fig. 10. Comparison of the full cell and corresponding combined half-cell results for entropy change. SOC values of the graphite half-cell are adjusted to correspond to the full cell graphite/LFP ratio.

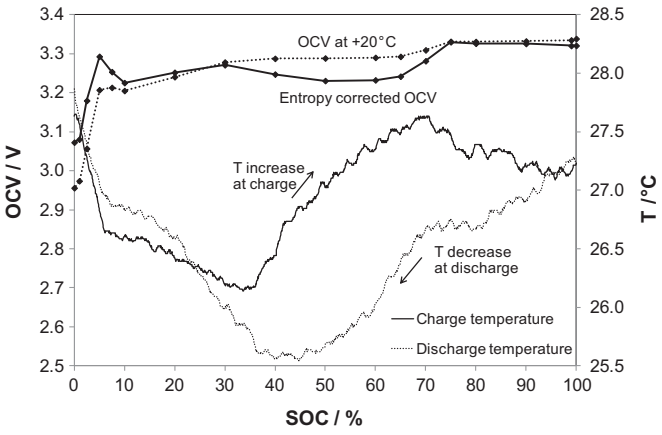

Fig. 11. Cell temperature at 0.1C constant current charge and discharge, entropy corrected OCV and OCV at +20 °C for the full cell.

$Q_{irreversible}$ in Equation (1) becomes insignificant, and $Q_{reversible}$ dominates. In the SOC range of 30–75%, the entropy corrected OCV is clearly lower than the OCV at +20 °C. The difference is due to the positive entropy change contribution. As discussed before, this entropy change behavior originates from the entropy change of the graphite electrode at the stage-2L ↔ stage-2-transition.

When the cell is discharged according to the above mentioned conditions inside this SOC range, the cell voltage is only slightly below the OCV and the difference between the cell voltage and entropy corrected OCV is absorbed as heat in the cell, and a cooling effect is observed. On the other hand, when the cell is charged, the cell voltage is much above the entropy corrected OCV and heat is produced. This phenomenon is seen in practice from the temperature curves in Fig. 11, where the cell indeed heats up in the charge direction and cools down in the discharge direction inside the 30–75% SOC range.

An opposite effect is seen in Fig. 11 at the SOCs of 0–10%, where the entropy change is negative and the corrected OCV is higher than OCV at +20 °C. When a low enough current is used, the cell produces heat when discharged and absorbs heat when charged. This effect is also seen in the temperature curves inside the SOC range of 0–10%.

LFP has a very moderate absolute entropy change value when compared to LCO [1,6,7] or lithium manganese oxide (LMO) [1,9] positive electrode materials. Thus also LFP/graphite cells have a smaller absolute entropy change and increased temperature stability vs. cells with LCO/graphite or LMO/graphite chemistries.

5. Conclusions

The thermal characteristics of an LFP-graphite commercial cell were divided into the contributions of the electrode materials. The changes in cell voltage as well as in the entropy change were both mostly determined by the corresponding graphite electrode values. The graphite electrode behavior was observed to be due to the staging phenomena and the changes in OCV and entropy change followed the two-phase coexistence ranges. The entropy change of the LFP electrode was measured to be almost constant over the whole SOC range. Possible single-phase areas causing sharp variations in the entropy change were not detected in this study.

Because of the graphite electrode entropy change behavior inside the stage-2L ↔ stage-2-transition, the full cell entropy change is positive and the cell absorbs heat when discharged at a low rate inside the SOC range of 30–75%. This cooling effect was also detected calorimetrically. The percentage range is not exactly the same for all commercial cells, as the graphite/LFP ratio varies depending on manufacturing.

Knowledge of the thermal characteristics is important in planning the battery cooling system and in predicting the cell heat generation at different SOCs. In practical applications, lots of cells are packed into a small volume very near to each other. This makes heat transfer very difficult and without a cooling system, efficient heat dispersion only takes place through the outer planes of the battery pack. The purpose of a cooling system is to maintain the cells at constant temperature. It should be sized to efficiently handle the extra heat produced due to the entropy effect inside the SOC range of 30–75% during charge and 0–10% during discharge. In addition, the battery degradation due to thermal stress can be reduced by restricting the SOC range of cycling to 100–10%. As concluded in this study, information about the cell internal resistance only is not enough to properly simulate the cell thermal behavior, but knowledge of the entropy effect is necessary.

Acknowledgments

We greatly thank European Batteries Ltd. for funding this work and providing the materials.

References

[1] V.V. Viswanathan, D. Choi, D. Wang, W. Xu, S. Towne, R.E. Williford, J.-G. Zhang, J. Liu, Z. Yang, J. Power Sources 195 (2010) 3720–3729.
[2] A. Yamada, H. Koizumi, S.-I. Nishimura, N. Sonoyama, R. Kanno, M. Yonemura, T. Nakamura, Y. Kobayashi, Nat. Mater. 5 (2006) 357–360.
[3] J. Dodd, Phase Composition and Dynamical Studies of Lithium Iron Phosphate (Ph.D. thesis), California Institute of Technology, 2007, pp. 75–94.
[4] Y. Reynier, R. Yazami, B. Fultz, J. Power Sources 119–121 (2003) 850–855.
[5] Y.F. Reynier, R. Yazami, B. Fultz, J. Electrochem. Soc. 151 (3) (2004) A422–A426.
[6] K.E. Thomas, J. Newman, J. Power Sources 119–121 (2003) 844–849.
[7] R.E. Williford, V.V. Viswanathan, J.-G. Zhang, J. Power Sources 189 (2009) 101–107.
[8] K. Takano, Y. Saito, K. Kanari, K. Nozaki, K. Kato, A. Negishi, T. Kato, J. Appl. Electrochem. 32 (2002) 251–258.
[9] K.E. Thomas, C. Bogatu, J. Newman, J. Electrochem. Soc. 148 (6) (2001) A570–A575.
[10] A.J. Bard, L.R. Faulkner, Electrochemical Methods, Fundamentals and Applications, second ed., J. Wiley & Sons, New York, 2001, pp. 47–48.
[11] V. Srinivasan, J. Newman, J. Electrochem. Soc. 151 (10) (2004) A1517–A1529.
[12] A.K. Padhi, K.S. Nanjundaswamy, J.B. Goodenough, J. Electrochem. Soc. 144 (4) (1997) 1188–1194.
[13] A.K. Padhi, K.S. Nanjundaswamy, C. Masquelier, S. Okada, J.B. Goodenough, J. Electrochem. Soc. 144 (5) (1997) 1609–1613.
[14] A. Yamada, S.C. Chung, K. Hinokuma, J. Electrochem. Soc. 148 (3) (2001) A224–A229.
[15] M. Winter, J.O. Besenhard, M.E. Spahr, P. Novák, Adv. Mater. 10 (10) (1998) 725–763.
[16] J.R. Dahn, Phys. Rev. B 44 (17) (1991) 9170–9177.